CELL BIOPHYSICS

Application of a Photosystem II Model for Analysis of Fluorescence Induction Curves in the 100 ns to 10 s Time Domain after Excitation with a Saturating Light Pulse

N. E. Belyaeva[a], V. Z. Pashchenko[a], G. Renger[b], G. Yu. Riznichenko[a], and A. B. Rubin[a]

[a] Department of Biophysics, Faculty of Biology, Moscow State University, Moscow, 119992 Russia;
fax 7 (495) 939 1115; e-mail: natalmurav@yandex.ru
[b] Max-Volmer Institute, Technical University, Berlin, 10623 Germany

Received February 1, 2006

Abstract—A mathematical model of photosystem II (PSII) events was used to analyze chlorophyll fluorescence transients in the time domain from 100 ns to 10 s after excitation with a saturating 10-ns flash, applied as a part of specialized illumination protocol, using preparations of a thermophilic strain of the unicellular green alga, *Chlorella pyrenoidosa Chick* (using both intact and diuron-treated cells). Analysis of simulation results has proven that particular attention should be given to flash-induced recombination processes, including nonradiative recombination in PSII, while subsequent charge transfer along the electron transport chain of thylakoid membrane can be adequately described by a single reaction of quinone reoxidation. The PSII model was extended by taking inhibition by diuron of the electron transport in the acceptor side of PSII into account, which allowed simulation of fluorescence induction curves observed in the presence of this inhibitor. The model parameters were determined (stromal pH, rate constants of nonradiative recombination, and the initial reduction state of the quinone pool) which provided adequate simulation of experimentally observed ratios of the maximal and initial fluorescence levels (F_m/F_0).

Key words: fluorescence induction, pulse fluorometry, electron transport, photosystem II, model simulation

INTRODUCTION

The intensity of chlorophyll fluorescence in photosynthesizing objects is determined by early events in the antenna complexes, by electron transport, and by slower processes in the photosynthetic membrane. Fluorescence changes can be observed in a time range from several picoseconds to tens of seconds. In order to measure fluorescence transients over a wide time range, special measurement protocols are applied, including excitation by continuous light or excitation with saturating light pulses of variable lengths on a background of continuous light of various intensities.

Mathematical modeling of the processes in the thylakoid membrane provides a means to formalize our view of events occurring in the photosynthetic membrane, to observe the kinetics of variables inaccessible to experimental determination, and to evaluate the rate constants of individual reactions through estimation of model parameters. The adequacy of the model can be judged by comparing the model variables with experimental kinetics of the respective parameters.

In experiments employing light of constant intensity, the induction curves of chlorophyll fluorescence are usually recorded in a time range from 50 μs to 100 s [1–9]. In order to simulate and analyze the fluorescence induction curves, mathematical models of variable complexity have been designed [6, 10–23]. The induction curves of chlorophyll fluorescence recorded under constant light in the time range from several milliseconds to seconds reflect the electron transport processes and generation of the transmembrane electric potential [12, 22–27]. At longer light exposures, the shape of the fluorescence induction curve depends also on formation of the electrochemical potential and is additionally linked to metabolic pathways consuming ATP and NADPH produced by primary photosynthetic events [2, 21, 22, 28].

The quantitative parameters of chlorophyll fluorescence, e.g., its relative quantum yield, are commonly used to characterize the physiological condition of pho-

Abbreviations: Chl—chlorophyll of the antenna and the reaction centers; DCMU—3-(3,4-dichlorophenyl)-1,1-dimethylurea; ETC—electron transport chain; FIC—fluorescence induction curves; Fl—chlorophyll fluorescence; H_L^+—protons of the thylakoid lumen; H_S^+—protons of the chloroplast stroma; OEC—oxygen-evolving complex; P680—chlorophyll of photosystem II reaction center; Phe—pheophytin; PSII—photosystem II; Q_A and Q_B—primary and secondary quinone acceptors of PSII; RC—reaction center; Y_Z—redox-active tyrosine of PSII.

tosynthesizing objects. Pulse fluorometry methods are widely applied for this purpose [6, 29].

The fastest fluorescence-related processes, with characteristic times up to 1 ns, occur in the light-harvesting antenna and in the neighborhood of the reaction center (RC). The reversible radical pair model has been used to describe fluorescence kinetics under the excitation of specimens by low-intensity laser flashes [4–6]. Within the framework of this model, the kinetics of prompt fluorescence decay in the time range below 1 ns was investigated. In addition, transient changes in probabilities (occupancies) were analyzed for photosystem II (PSII) states formed by the reaction center chlorophyll P680, pheophytin (Phe), and the primary quinone acceptor Q_A [10, 30–36].

In the time range above 1 ns, the contributions of individual states of PSII reaction centers to the recorded signals of prompt fluorescence and delayed (recombination) fluorescence were analyzed through careful consideration of electron transfer steps related to P680$^+$ reduction and Q_A^- reoxidation in the pigment–protein complex of PSII [37–39]. In PSII preparations where the oxygen-evolving complex (OEC) is intact, the tyrosine Y_Z electron donor immediately reduced the photoactive pigment P680$^+$ within tens of nanoseconds [39]. The emerging state Y_Z^{OX}P680Q_A^- remains dominant within several microseconds after the actinic flash owing to low rates of Y_Z^{OX} and Q_A^- recombination (~100 µs) [3] and because of slow electron transfer to Q_B (~200 µs) [39]. The subsequent reduction of Y_Z^{OX} within a few microseconds after the flash is determined by characteristic lifetimes of S_i-states in the OEC cycle [39].

In order to analyze the reaction of the first OEC cycle in response to a short flash, the sample should be excited with a powerful saturation pulse inducing simultaneous oxidation of P680$^+$ for all PSII complexes. The recording system developed by Christen et al. [37] allowed the delayed fluorescence to be analyzed in the time range from 100 ns to 5 µs. In more recent versions of the measuring instrument, the recording time limit was extended to 10 s.

The complex of charge transfer and recombination events in PSII could be analyzed in detail with a mathematical model providing adequate kinetic simulation of the processes in the donor and the acceptor sides of PSII. By changing the model parameters, it is possible to simulate electron transfer in PSII under the action of various agents and analyze the delayed fluorescence data in samples treated with various inhibitors, 3-(3,4-dichlorophenyl)-1,1-dimethylurea (DCMU) in particular.

In this work, a theoretical and experimental investigation of electron transfer in PSII was performed. Experimental measurements of fluorescence signals excited with a saturating flash of 10 ns duration were performed for untreated and DCMU-treated prepara-

tions in the time range from 100 ns to 10 s using a specialized recording system developed in the Renger laboratory [30]. The experimental data were analyzed by means of a mathematical model of events occurring in PSII. The PSII model represents the detailed version of the PSII section in the generalized model of primary photosynthetic events (the thylakoid model) developed at the Biophysics Department (Faculty of Biology) of Moscow State University [19–23]. The thylakoid model takes a complex of charge transfer steps in the thylakoid membrane into account and adequately describes the complete induction curve of chlorophyll fluorescence with the characteristic features of the increase and decrease of the fluorescence signal (O–J–I–P–S–M-T transients) observed [5] under continuous illumination in the time range from 40 µs to 10 s, both at high and low light intensities [22].

In this study, a detailed model of PSII was used to analyze the contribution of PSII individual states to fluorescence kinetics after excitation with a light pulse of nanosecond duration. It is shown that the kinetics of fluorescence induction could be adequately modeled by considering recombination processes, including nonradiative recombination in PSII, while subsequent charge transfers along the electron transport chain (ETC) of thylakoid membrane can be treated in a simplified manner by considering them as one reaction of quinone reoxidation. This version of the PSII model accounts for the competitive inhibition by DCMU of electron transport in the PSII acceptor side, which allowed us to simulate the experimental kinetic curves observed in the presence of this inhibitor.

MATERIALS AND METHODS

Fluorescence measurements after pulse excitation. A culture of unicellular green alga *Chlorella pyrenoidosa Chick* (thermophilic strain CALU-175 S-39) was used in the experiment. The alga culture was grown on the 20% strength Kamiya medium in cylindrical glass vessels at 37°C under illumination with fluorescent lamps (irradiance of 30 W/m^2 at the level of vessel surface) and continuous aeration. The concentration of cells sampled for the experiment was about 5×10^6 cell/ml.

Transient flash-induced changes of fluorescence yield (Fig. 1) were measured in the time range from 100 ns to 10 s using the experimental setup described in [38]. The sample in the cuvette was excited with a single-turnover flash (λ_{act} = 532 nm, 10 ns width). The pulse energy was 0.4 mJ/cm^2, which ensured 100% excitation of RCs in all cells (saturating pulse). The flash-induced changes of fluorescence relative quantum yield (induction curves) were recorded by means of weak measuring light obtained from a light-emitting diode (LED) array (Toshiba TLRA 190P) providing periodic light pulses at λ_{meas} = 600 nm. Fluorescence was recorded with an R5916 U-51 multichannel plate photomultiplier tube (MCP-PMT, Hamamatsu). The

$F(t)/F_0$
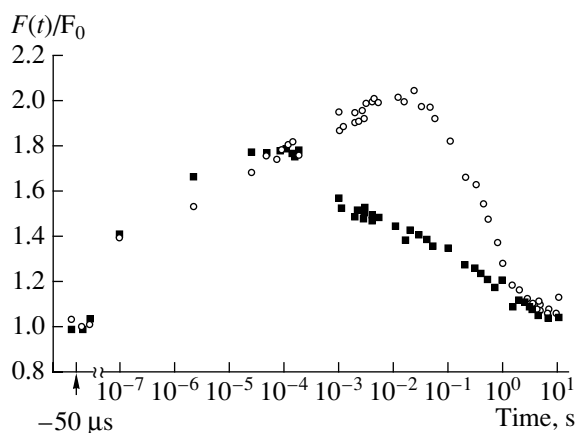
Fig. 1. Experimental measurements of fluorescence induction curves in the time range from 100 ns to 10 s with the cell culture of green alga *Chlorella pyrenoidosa Chick*, thermophilic strain CALU-175 S-39 in the absence of inhibitors (squares) and in the presence of DCMU (circles) after preliminary detection of F_0 fluorescence (at $t = -50$ μs) and subsequent exposure to saturating flash with a duration of 10 ns. Square symbols represent fluorescence of untreated (control) cells; circles, the treatment with 5 μM DCMU.

MCP-PMT device could be gated with $\tau \sim 1$ ns and had a signal to noise ratio (open/closed state) of 1.7×10^8. The initial F_0 fluorescence level was determined with a measuring light beam applied 50 μs before the excitation by the actinic flash. The incidence of weak measuring light provided from LED array was synchronized with the gate function of the MCD-PMT via a DS-345 pulse generator (Stanford Research System). The fluorescence records acquired before and after each laser flash were stored in a computer. The signal to noise ratio was improved by sampling and averaging 80 individual kinetic curves. In order to prevent photodamage, the cell suspension was continuously pumped through the measuring cuvette.

Description of the PSII model. Figure 2 shows the scheme of PSII RC states and their mutual transitions adopted in the model [20–22]. The scheme includes kinetic states involved in the primary charge separation (reactions 2, 9, 16, and 29), stabilization of separated charges (reactions 3, 4, 10, 11, 17, 18, 30, and 31), charge transfer to the quinone pool (PQH$_2$) associated with emptying of the Q$_B$ site (reactions 7, 14, and 21–27) and the subsequent refilling of empty Q$_B$ site with oxidized quinones (PQ) (reactions 34–40). We assumed that each electron transfer from OEC to oxidized P680$^+$ (designated as Chl+ in the scheme) (reactions 4, 11, 18, and 31) was accompanied by the release of one proton into the thylakoid lumen.

The chlorophyll (Chl) transition to the excited state, Chl* is given by the excitation rate constant in light pulse $k_L = k_i$, $i = 1, 5, 8, 12, 15, 19, 28,$ and 32 (where i is the reaction number in PSII scheme shown in Fig. 2). The number of light quanta absorbed by RC per second

($k_L = 1500$ s^{-1}) corresponded to an irradiance of 1000 W/m^2 (at 600 nm). The reverse process, Chl* decay is accompanied by fluorescence emission with the rate constant $k_F = k_{-i}$. The fluorescence yield was calculated by multiplying the sum concentration of all PSII fluorescent states into the ratio of rate constants k_F/k_L:

$$F = \frac{k_F}{k_L}(x_2 + y_2 + z_2 + g_2 + x_6 + y_6 + z_6 + g_6). \quad (1)$$

In our analysis of isolated PSII model, the values of proton concentrations in the stroma and lumen ($[\mathrm{H_S^+}]$ and $[\mathrm{H_L^+}]$, respectively) and the transmembrane electric potential $\Delta\Psi$ were taken as parameters. The influence of $\Delta\Psi$ was taken into account for electron transfer reactions directed perpendicular to the membrane surface:

$$\tilde{K}_{eq} = \exp(nF/RT\Delta E_m - F/RT\alpha_I\Delta\Psi), \quad (2)$$

where ΔE_m is the difference of midpoint redox potential of electron carriers [40] and α_i is electrogenicity factor, i.e., the portion of the transmembrane $\Delta\Psi$ that affects the reaction rate [41]. It should be noted that the detailed models of PSII processes published to date [13, 15] do not take into account the dependence of electron transport rate constants on $\Delta\Psi$.

The reoxidation of the mobile carrier PQH$_2$ was described by a single reaction (V_{41} in Fig. 2). In order to describe the events occurring within the PSII model, a matrix of rate constants was composed for the transitions between individual states of the complex. Thus, we obtained a set of 30 ordinary differential equations describing the concentrations of PSII complex in various redox states and of plastoquinone stromal forms (PQH$_2$ and PQ).

The differential equation for any ith component was written as:

$$dX_i/dt = v_{in}(X_i) - v_{out}(X_i),$$

where X_i is the concentration of ith component expressed in mM and $v_{in}(X_i)$ and $v_{out}(X_i)$ designate total rates of this component production (inflow) and consumption (outflow) in mM/s. Concentrations of various PSII states were calculated as the product of the probability for a given state and the total concentration of PSII complex in the system. The interaction of the PSII complex with the mobile carriers was described according to the mass action law assuming a bimolecular reaction [22].

We assumed that the concentration of PSII complex in the thylakoid membrane is 1.62 mM, while the concentrations of PSII complex and the pool quinones are in the ratio of 1 : 6 [42]. The redox state concentrations of individual electron carriers in the PSII reaction center were calculated as a sum concentration of all PSII states with the given redox state of the electron carrier.
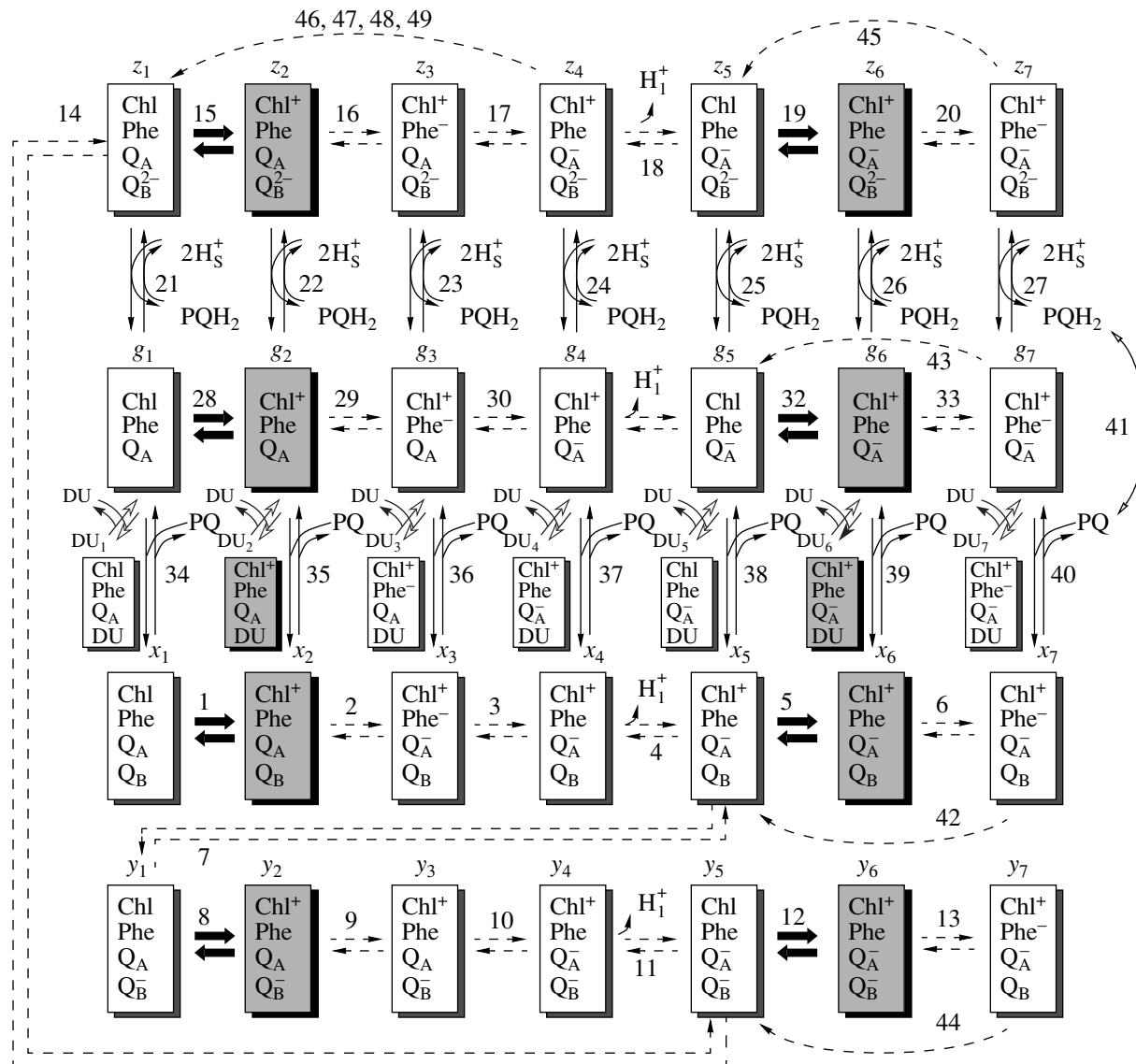
Fig. 2. Scheme of the catalytic cycle of photosystem II. Each rectangle represents one of the kinetic states of PSII, specified by the redox states of constituent electron carriers. Shaded rectangles indicate the excited states capable of emitting fluorescence. Chl designates the total chlorophyll of PSII including P680 and the antenna pigments. Phe is the primary electron acceptor pheophytin. Q_A and Q_B are the primary and secondary quinone acceptors. PQ and PQH_2 designate plastoquinone and plastoquinol, respectively. H_L^+ and H_S^+ designate protons released into the lumen and absorbed from the stroma, respectively. Dashed arrows designate fast steps (with characteristic times shorter than 0.1 ms); solid arrows mark slow stages (with characteristic times equal to or longer than 1 ms); wide arrows mark the light steps. Numbers near the arrows correspond to the reaction numbers. Letters above the rectangles ($x_i, y_i, z_i, g_i, du_i, i = 1, ..., 7$) correspond to the model variables. Small boxes in the row containing du_i variables designate the states with the Q_B site occupied by the inhibitor (DCMU). The inhibitor molecule (DU) occupies the empty Q_B site and forms du_i states incapable of electron transfer from the primary to the secondary quinone. Dashed arcs designate nonradiative recombination of Phe^- with $P680^+$ (reactions 42–45) and of Q_A^- with $P680^+$ (reactions 46–49).

For example, the concentration of PSII states with the reduced Q_A^- is given by the formula:

$$\sum_{i=4}^{7} ([x_i] + [g_i] + [y_i] + [z_i]). \qquad (3)$$

The term "forms" is used to designate different types of PSII states. For example, the term "fifth forms" (x_5, g_5, y_5, z_5) designates the set of PSII states where the electron is stabilized on Q_A^-.

The present version of the PSII model, unlike the previous one [20–22], includes two types of irreversible
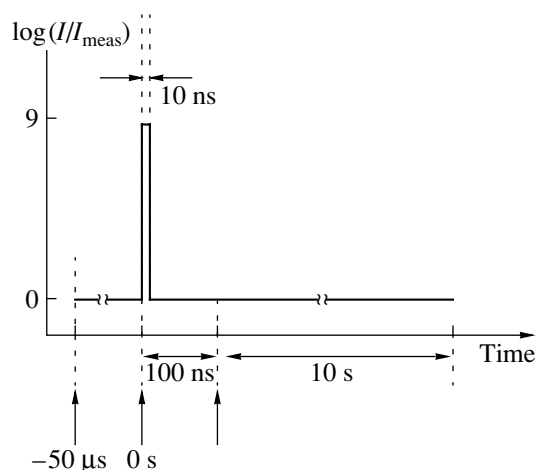
Fig. 3. Timing scheme of the experiment specifying illumination modes used for fluorescence measurements shown in Fig. 1. Arrows along the horizontal axis mark the moments when the illumination modes were switched over. The vertical axis shows the logarithm of light intensities used in the model to simulate effects induced by measuring light and saturating flash.

nonradiative recombination, which are designated in the scheme with dashed arced arrows.

The negative charge of reduced pheophytin recombines with oxidized chlorophyll in the closed RC. These reactions (42–45) are incorporated into the model as transitions of the seventh forms to the fifth forms with the rate constants specified in the discussion.

The reduced primary quinone Q_A^- can recombine with oxidized electron donors, i.e., with RC chlorophyll, redox-active tyrosine, or OEC S-states. These nonradiative recombination events are indicated in the model by transitions from the fourth forms to the first forms (reactions 46–49, recombination of Q_A^- and $P680^+$) with rate constants ranging from 200 to 2000 s^{-1}.

The inhibition of electron transfer to the quinone pool was described in the model in two different ways. In the first approach, we reduced the rate constants of electron transfer to Q_B in the same manner as described in the literature [13, 15]. The second approach allowed us to take into account the concentration of the inhibitor applied. To this end, we introduced additional reactions describing the interaction between DCMU and the empty Q_B site (g_i) (Fig. 2). Thus, the scheme of PSII states has been supplemented by an additional (horizontal) row consisting of seven states (du_i). We assumed that the presence of DCMU molecule in the Q_B site allows the PSII catalytic cycle to undergo transformations corresponding to horizontal arrows in the scheme lines (Fig. 2).

Experiment scheme. The experimental data in Fig. 1 were obtained at the time point –50 μs before saturating

single-turnover flash and then for a number of points in the time range from 100 ns to 10 s after the flash. Square symbols refer to untreated cells and circles correspond to DCMU-treated cells. The scheme of the experimental protocol is shown in Fig. 3. Prior to single-turnover flash, the sample was illuminated with weak measuring light for 10 s (not shown in Fig. 3). Fifty microseconds before the flash (the point designated as –50 μs in Fig. 3), fluorescence intensity was recorded as a measure of F_0 value. A saturating single-turnover flash with a length of 10 ns ($t_1 = 0$, $t_2 = 10$ ns) excited all reaction centers. Measurements of fluorescence after the flash (the induction curve) were started at 100 ns ($t_3 = 100$ ns) and continued until 10 s ($t_4 = 10$ s).

CALCULATION RESULTS

1. Assessment of the system condition before and after the flash. The processes in PSII occurring under various illumination conditions were simulated in several steps. The table lists calculated concentrations of individual PSII states in intact and DCMU-treated samples at the reference time points, i.e., when the measuring light was switched on after dark adaptation, when F_0 was measured (–50 μs), and at the moment of first measurement after the flash ($t_3 = 100$ ns).

1.1. Effect of measuring light. Before the onset of measuring light, the distribution of PSII concentrations is determined by conditions of dark adaptation when the values of light-dependent constants equal zero in the PSII model. Under these conditions, only neutral states x_1 and g_1 are populated (table, first column). The proportion of their concentrations is determined by the parameters of interaction between the PSII acceptor side and the mobile molecules of the quinone pool.

The effect of the applied measuring light was simulated by assigning the value of light constant $k_L = 0.6$ s^{-1}, which corresponds to irradiance of 0.4 W m^{-2}. Using these values, we calculated the kinetic curves for fluorescence induction (Fig. 4, curve *1* Fl) and for the concentration of PSII states with open RCs (curves *3, 5* Q_A). For comparison, we simulated the effect of high intensity actinic light ($k_L = 6000$ s^{-1}); the results are also plotted in Fig. 4 (curve *2* Fl and curves *4, 6* Q_A).

In the case of weak measuring light, the steady-state level of fluorescence induction curve (Fig. 4, *1* Fl) at exposure times $t > 1$ s was higher than the initial value F_0 by a factor of 0.15. The model of PSII predicted that, upon long (10 s) exposure to weak measuring light, the states with open RCs are being populated (Fig. 4, curves *3, 5* Q_A). In this case, 35% of dark-adapted PSII states with oxidized or empty Q_B site ($x_1 + g_1$, Fig. 4, *3* $Q_A Q_B$) were converted to open RC states with the reduced secondary quinone ($y_1 + z_1$, Fig. 4, *5* $Q_A Q_B^{(2)-}$). The respective values of variables are listed in table columns 2 and 3. We assumed that these values describe PSII of the samples preadapted in darkness and brought

Concentrations of the redox states as calculated by modeling the PSII processes in the absence and presence (5 μM) DCMU

Experimental conditions, parameters, and redox states of the PSII model	Sample was dark-adapted ($k_L = 0$) and then exposed to weak measuring light ($k_L = 0.6$ s^{-1}) for determination of F_0		First measurement after the flash: $k_L = 6 \times 10^8$ s^{-1} in the period from $t_1 = 0$ to $t_2 = 10$ ns and $k_L = 0.6$ s^{-1} thereafter until $t_3 = 100$ ns		Condition established by the end of the flash: this was taken as the starting condition for calculation of the induction curves, $t_3 = 100$ ns	
	dark adaptation	weak light, 50 μs prior to the light pulse	$t_3 = 100$ ns after the light pulse			
$x1$	0.82	0.45523	0.79165	0.1015	0.09306	0.1	0.1
$x2 \times 10^{-8}$	0.0	0.0137	0.02	0.01	0.03	0.0	0.0
$x4$	0.0	0.00029	0.00089	0.34981	0.69727	0.4	0.68
$x5$	0.0	0.02739	0.08806	0.03161	0.08824	0.03	0.08
$x6 \times 10^{-8}$	0.0	0.00393	0.013	0.001	0.0076	0.0	0.0
$g1$	0.8	0.48957	0.16729	0.10915	0.02003	0.2	0.02
$g2 \times 10^{-8}$	0.0	0.0147	0.004	0.01	0.007	0.0	0.0
$g4$	0.0	0.00032	0.00019	0.37618	0.15011	0.38	0.15
$g5$	0.0	0.02948	0.01861	0.03403	0.01856	0.04	0.019
$g6 \times 10^{-8}$	0.0	0.00423	0.0027	0.0001	0.0016	0.0	0.0
$y1$	0	0.54648	0.17608	0.12118	0.02073	0.12	0.033
$y2 \times 10^{-8}$	0.0	0.0164	0.0046	0.01	0.007	0.0	0.0
$y4$	0.0	0.00001	0.00004	0.41966	0.15522	0.42	0.15
$y5$	0.0	0.00624	0.00242	0.03403	0.00228	0.01	0.002
$y6 \times 10^{-8}$	0.0	0.00089	0.0003	0.0001	0.0002	0.0	0.0
$z1$	0	0.06119	0.0023	0.01364	0.00026	0.0	0.0
$z2 \times 10^{-8}$	0.0	0.00184	0.00006	0.0001	0.00009	0.0	0.0
$z4$	0	0.00004	0.0	0.04702	0.00194	0.0	0.0
$z5$	0	0.00369	0.0002	0.00406	0.0002	0.0	0.0
$z6 \times 10^{-8}$	0.0	0.00053	0.00003	0.00001	0.00002	0.0	0.0
$du1$	0.0	0	0.33073	0	0.03897	0.0	0.04
$du2 \times 10^{-8}$	0.0	0	0.0086	0	0.014	0.0	0.0
$du4$	0.0	0.0	0.00041	0.0	0.29202	0.0	0.296
$du5$	0.0	0	0.04104	0	0.04111	0.0	0.05
$du6 \times 10^{-8}$	0.0	0	0.006	0	0.0035	0.0	0.0
		DCMU		DCMU		DCMU

into condition with the initial fluorescence F_0 at $t = -50$ μs prior to the saturating flash. For comparison, a classical induction curve of chlorophyll fluorescence is shown in Fig. 4. This calculated curve describes the multiphase fluorescence increase (O–J–I–P transients) recorded after switching on the high-intensity light (Fig. 4, 2, Fl) [5, 22]. It shows that variable fluorescence increases from the initial (F_0) level to its peak within ~100 ms, while the concentration of open RCs decreases by a factor of 500 (Fig. 4, curves 4, 6 Q$_A$).

1.2 Effect of single-turnover flash. The effect of a saturating light pulse was simulated by assuming that $k_L = 6 \times 10^8$ s^{-1} (light intensity of 4×10^8 W/m^2) for the time interval 0–10 ns and that $k_L = 0.6$ s^{-1} in the period from 10 ns to 100 ns. The calculated concentrations of

PSII states arising after the action of strong light pulse are listed in table columns 4 and 5. The simulation showed that 100 ns after the onset of saturating 10-ns pulse, the states with oxidized RC chlorophyll P680$^+$ (the forth forms) were predominant. The occupancies of the fourth forms ($x_4 + g_4 + y_4 + z_4$) amounted to 71% and 80% for the untreated and DCMU-treated samples, respectively.

2. Fluorescence yield transients after the light pulse. The values of model variables (table, columns 4 and 5) obtained for the time instant $t_3 = 100$ ns were corrected to obtain the best fit of theoretical and experimental data. The final values of the variables (table columns 6 and 7) were used as the starting values for simulation of fluorescence changes after the light
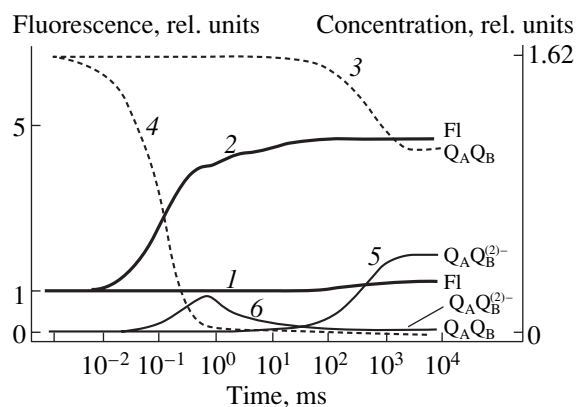
Fig. 4. Simulation of the effects of continuous light switched on after dark adaptation. Curves *1*, *3*, and *5* were calculated for weak measuring light (light constant $k_L = 0.6\ \mathrm{s}^{-1}$); curves *2*, *4*, and *6* were calculated for the actinic light pulse of saturating intensity ($k_L = 6 \times 10^3\ \mathrm{s}^{-1}$). (*1*, *2* Fl) Fluorescence induction; (*3*, *4* $Q_A Q_B$) the concentration of open RCs with oxidized Q_B (x_1 and g_1); (*5*, *6* $Q_A Q_B^{(2)-}$) the concentration of open RCs with one electron (y_1, $Q_A Q_B^-$) and two electrons (z_1, $Q_A Q_B^{-2}$) on the secondary quinone.

Fig. 5. Theoretical curves obtained for the initial conditions simulating the action of high-intensity nanosecond pulse (light constant $k_L = 6 \times 10^8\ \mathrm{s}^{-1}$) applied after measuring light ($k_L = 0.6\ \mathrm{s}^{-1}$). The calculation was performed under the assumption of weak measuring light ($k_L = 0.6\ \mathrm{s}^{-1}$) using the model parameters specific for the untreated sample (solid line) and DCMU-treated sample (dashed line). The simulated curves are compared with experimental data for the untreated sample (solid squares) and DCMU-treated sample (open circles).

pulse. The calculations were performed assuming that $k_L = 0.6\ \mathrm{s}^{-1}$ (measuring light on) for the time range from 0 to 10 s. Figure 5 compares the calculated and experimental curves in the time range from 100 ns to 10 s for intact and DCMU-treated cells. The simulated fluorescence kinetics for preparations in the absence and in the presence of 5 μM DCMU are shown with solid and dashed curves, respectively. A good fit of experimental and theoretical curves is evident.

2.1. The phase of fluorescence increase. Under control conditions, the fluorescence intensity reaches its peak at about 50 μs (solid theoretical curve and experimental data (square symbols)). In the presence of DCMU, the fluorescence increase takes longer and peaks at about 10 ms (dashed theoretical curve and experimental data shown with circles). The maximal fluorescence yield scaled to the initial F_0 value was in accordance with experimental data and equaled $1.8F_0$ and $2.1F_0$ for the untreated and DCMU-treated samples, respectively.

2.2. The phase of fluorescence decay. In experiments with untreated cells of thermophilic unicellular alga *Chlorella pyrenoidosa* Chick, the fluorescence decay in the time range above 100 μs comprised three phases, with the stationary fluorescence level close to F_0. During the first phase in the time domain up to 1 ms, the fluorescence signal decreased by 45%. The second phase extended to about 100 ms and accounted for a signal decrease by ~20%. During the third phase (within the period of 1–10 s) the signal decreased by 35%. The theoretical curve provided a good approximation of the

second and third phases, with incomplete correspondence to the first phase.

The fluorescence decay observed in the presence of DCMU in the time range from 100 ms to 1 s was described by a single-phase "diuron-type" curve (Fig. 5, dashed line).

In general, the suggested model of PSII provides adequate description for diverging kinetic curves of fluorescence induction in the untreated and DCMU-treated cells (Figs. 1, 5). In the sections below we address the question of how the kinetic characteristics of calculated curves are affected by changes of the model parameters.

3. Modeling of PSII processes in intact (control) samples. While modeling the fluorescence transients in untreated samples, an adequate set of model parameters was established by adjusting parameters of electron transport in the donor and acceptor sides of PSII (Fig. 6).

3.1. The rate of chlorophyll reduction in the reaction center. The operation of OEC was not considered in detail in the PSII model; instead, we used an averaged characteristic of OEC functioning $k_{OEC} = k_i$ ($i = 4, 11, 18$, and 31; Fig. 2). It is known that tyrosine reduces the RC chlorophyll with rate constants ranging from 3×10^6 to $10^9\ \mathrm{s}^{-1}$ depending on the stage of S_i cycle, while the OEC complex reduces tyrosine with rate constants of 10^3–$3 \times 10^4\ \mathrm{s}^{-1}$ [42]. Experimental data obtained with intact cells (squares) were fit to the solid curve in Fig. 5 using $k_{OEC} = 10^7\ \mathrm{s}^{-1}$. The results shown in Fig. 6a were calculated for two k_{OEC} values: $5 \times 10^4\ \mathrm{s}^{-1}$ (curve *1*) and $10^7\ \mathrm{s}^{-1}$ (*2*). In the time scale below 10 μs, the theo-

retical curves calculated with $k_{OEC} = 10^7$ s^{-1} adequately described the fluorescence increase. The theoretical curve reached its peak within less than 40 μs. In the experiment, the fluorescence peak was observed at 45–100 μs (Fig. 1, squares and [2]). In the model such an increase time was obtained with $k_{OEC} = 100–150$ ms^{-1}, which is faster than any stage of tyrosine reduction in the OEC cycle but is slower than the rate of chlorophyll reduction by tyrosine.

The PSII states with oxidized RC chlorophyll (the fourth forms, P680$^+$) are predominant at $t_3 = 100$ ns after the pulse onset (table columns 4 and 5). The curves 1 and 2 Chl$^+$ (Fig. 6a) show that a 1000-fold drop in the concentration of the fourth forms in the time range below 1 μs (100 μs) with the allowance of $k_{OEC} = 5 \times 10^4$ s^{-1} (10^7 s^{-1}) occurred in parallel with an increase to the peak concentration of the fifth forms (forms with reduced RC chlorophyll; i.e., the sum $x_5 + g_5$, curves 1, 2 $Q_A^- Q_B$, Fig. 6a).

The increase in the number of states with electrons stabilized at Q_A^- corresponded to the fluorescence increase to the peak. Thus, the acceleration of the process rates on the donor side of PSII resulted in a faster increase of chlorophyll fluorescence and had no influence on the decay of the induction curve (up to 10 s).

3.2. Electron transfer in the acceptor side of PSII and in the quinone pool. It is assumed [4, 38] that the fluorescence decay phases result from electron transfer into the quinone pool. According to the scheme of the PSII catalytic cycle (Fig. 2), the concentration of protons in the chloroplast stroma $[H_S^+]$ significantly influences the reaction emptying the Q_B site with doubly reduced quinone Q_B^{2-} (z_i, $i = 1, …, 7$). With our model we investigated the effect of stromal pH in the physiological range (pH 7–8) and found that the parameters of the quinone pool become increasingly important at high stromal pH for the description of the fluorescence decay. The curves in Fig. 6b were calculated at proton concentration in the stroma $[H_S^+] = 5 \times 10^{-5}$ mM, which is equivalent to the stroma pH of 7.3.

The initial reduction state of the quinone pool estimated from modeling of the measuring light effect (i.e., for the PSII state with the fluorescence F_0) was equal to 0.25%. This was considered to be the lowest possible value; the inclusion of this value in further calculations yielded the kinetic curves 1 in Fig. 6b. When we increased the initial fraction of reduced quinones in the pool to 12.5%, we obtained curves 2 showing lower amplitude of the fluorescence decay during the first phase (2, Fl) compared to the experiment.

The reaction of quinone reoxidation, designated in the model as reaction 41 (Fig. 2), describes the complex of processes occurring in ETC after electron transfer in PSII. When we kept the assumed extent of pool reduction at 12.5% and reduced the rate constant for quinol
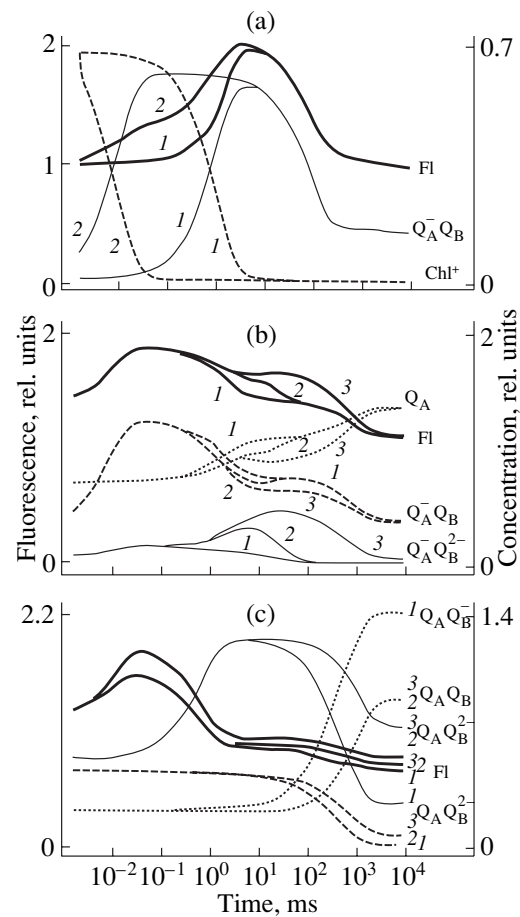
Fig. 6. Theoretical curves obtained for the initial conditions simulating the action of high-intensity nanosecond pulse (light constant $k_L = 6 \times 10^8$ s^{-1}) applied after weak measuring light ($k_L = 0.6$ s^{-1}). The curves were calculated under assumption of weak measuring light conditions ($k_L = 0.6$ s^{-1}) and the model parameters specific for the untreated sample (control conditions). Fl—fluorescence induction; Chl$^+$—concentration of PSII redox states with oxidized RC chlorophyll (the sum of the fourth forms, x_4, g_4, y_4, z_4); PQH$_2$—plastoquinol concentration. Open RCs with reduced chlorophyll are designated as $Q_A Q_B$ (the sum of x_1 and g_1) and $Q_A Q_B^{(2)-}$ (the sum of y_1 and z_1); closed RCs with reduced chlorophyll are designated as $Q_A^- Q_B$ (the sum of x_5 and g_5) and $Q_A^- Q_B^{(2)-}$ (the sum of y_5 and z_5). (a) Kinetic curves obtained with two values of rate constants (k_i, $i = 4, 11, 18, 31$) for the reduction of oxidized RC chlorophyll (P680$^+$): 10^5 s^{-1} (curves 1) and 10^7 (curves 2). (b) Kinetic curves 1, 2, and 3 were obtained by assuming an extent of the quinone pool reduction equal to (1) 0.25%, (2) 12.5%, and (3) 12.5% and by assigning the rate constant of quinol reoxidation equal to (1) 50 s^{-1}, (2) 50 s^{-1}, and (3) 5 s^{-1}. (c) The sets of kinetic curves 1 and 2 were obtained by decreasing the rate constant of nonradiative recombination of Q_A^- and P680$^+$ from 2000 s^{-1} to 200 s^{-1} with the provision that the rate constant of nonradiative recombination of Phe$^-$ and P680$^+$ equals to 10^5 s^{-1} (curves 1 and 2) or 10^4 s^{-1} (curves 3).

reoxidation by a factor of 50 (from 100 to 2 s^{-1}), we did not observe the second phase of the fluorescence decay (curve *3* Fl, Fig. 6b).

The kinetic features of the fluorescence curves are determined by the contributions of PSII states shown in Fig. 6b: open states ($x_1 + g_1 + y_1 + z_1$) with Q_A in oxidized form, closed states ($x_5 + g_5$) corresponding to $Q_A^- Q_B$, and closed states ($y_5 + z_5$) corresponding to $Q_A^- Q_B^{(2-)}$. Regardless of the parameters chosen, the maximal fluorescence level is determined by the contributions of closed states with oxidized Q_B ($Q_A^- Q_B$, $x_5 + g_5$). Both the increase in the reduction of the quinone pool (transition from curves *1* to curves *2*) and the retardation of plastoquinol reoxidation (transition to curves *3*) elevated the concentration of closed states (curves $Q_A^- Q_B^{(2-)}$).

Analysis of our modeling results allowed us to estimate the extent of pool reduction characteristic of the initial fluorescence level (0.25%). We identified the parameters that ensure optimal fit to experimental data; i.e., stromal pH equal to 7.3 and a rate constant for quinol reoxidation ranging from 10 to 100 s^{-1}.

3.3. Nonradiative recombination processes. The calculated values of the fluorescence peak and the final level approaching F_0 in 10 s after the light pulse depended essentially in the model on the parameters of nonradiative recombination (Fig. 6c).

In the case where recombination of Q_A^- with oxidized donors (P680$^+$, reactions 46–49) was comparable in terms of reaction rates (curves *1*) with the electron transfer rates from Q_A^- to Q_B (hundreds of microseconds), the electron transfer to Q_B in the acceptor side did not compensate, already at the end of 1 ms, for the electron removal from the quinol pool resulting from quinone reoxidation (curve *1* PQH$_2$, Fig. 6c). Accordingly, upon the PSII transition to a state with the initial fluorescence characteristic of an open RC during the third phase, the first forms with oxidized Q_B were predominant (curve *1* $Q_A Q_B$ for the sum $x_1 + g_1$). In the case when the rate constant for recombination k_i ($i = $ 46–49) was lower than the rate constant for the electron transfer to Q_B, the PSII acceptor side accumulated electrons (curve *2*, $Q_A Q_B^{(2-)}$). Consequently, during the transition from curves *1* to curves *2*, the fluorescence in the third phase was high in the time range of seconds, and the extent of pool reduction was comparatively high (*2*, PQH$_2$).

The transition from kinetic curves *2* to curves *3* in Fig. 6c was achieved by decreasing the rate constant k_i for recombination of Phe$^-$ with P680$^+$ ($i = $ 42, 43, 44, and 45) from 10^5 to 10^4 s^{-1}. This replacement increased the fluorescence yield (curve *3* Fl) at all stages of fluorescence increase and decay except for the initial and final levels. The model showed that this increase was due to the increased probabilities of doubly reduced stages with electrons localized on pheophytin and the primary quinone (the seventh column in Fig. 2). The kinetic curves of these states resembled the time course of fluorescence intensity (curves *2*, *3* Fl, Fig. 6c). The concentration (probability) of the fifth and seventh forms had an effect on the number of excited closed states of PSII reactions centers (sixth forms) whose emission accounts for the increased fluorescence level compared to the initial level.

Thus, the model shows that the processes of nonradiative recombination determine both the fluorescence maximum and the F_0 level achieved during transition to the stationary state. The increase in the rate of nonradiative recombination of pheophytin in the closed RC decreases the probability (occupancy) of doubly reduced states with electrons located on pheophytin and on the primary quinone (seventh states, Fig. 2). In this case, the process of electron transfer to the pool was not affected, and kinetics of the pool reduction (curves *2*, *3*, PQH$_2$) turned out to be identical for the calculation procedures 2 and 3.

4. Simulation of PSII processes in DCMU-treated samples. The calculations presented in Fig. 7 show that the modified PSII model describing DCMU binding to empty Q_B site allows optimal fitting of theoretical results to experimental data recorded in the presence of DCMU (Fig. 1, circles).

As seen in Fig. 7a, an increase in DCMU concentration (from 5 to 50 µM) elevated both the fluorescence increase time and the peak value of fluorescence (transition from curve *1* to curve *2* Fl). This was caused by the increase in concentration of PSII kinetic states with Q_B site occupied by the inhibitor molecule (transition from *1* to *2* Q_A^- DCMU). The contribution of closed and open PSII states with oxidized Q_B ($Q_A^- Q_B$ and $Q_A Q_B$) was only significant for the peak fluorescence level, while during transition to the stationary state it decreased by 4–5 orders of magnitude compared to the contribution of the states where the Q_B site was occupied by the inhibitor (curves Q_A^- DCMU). The contribution of PSII states with reduced Q_B can be neglected as a very small one.

The results displayed in Fig. 7c for the two values of rate constants of nonradiative recombination of Q_A^- and P680$^+$ prove that characteristics of the multiphase fluorescence decay in the "diuron-type curve" are determined by recombination of PSII with the Q_B site occupied with the inhibitor molecule (Q_A^- DCMU). The enhancement of recombination between Q_A^- and P680$^+$ (an increase in the rate constant from 200 to 400 s^{-1})
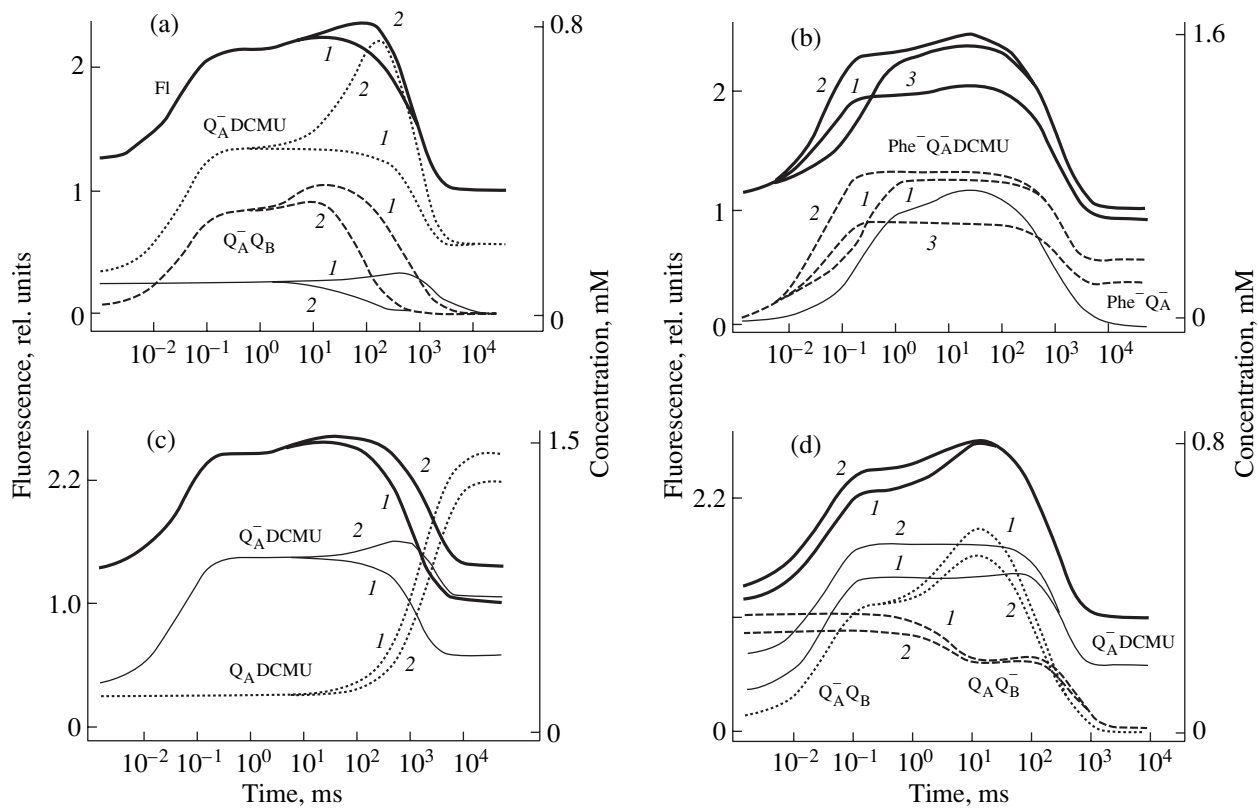
Fig. 7. Theoretical curves obtained for the initial conditions simulating the action of a high-intensity nanosecond flash (light constant $k_L = 6 \times 10^8$ s^{-1}) on the background of measuring light ($k_L = 0.6$ s^{-1}) in samples treated with 5 µM DCMU. Fl—fluorescence induction. Concentration of open reaction centers, $Q_A Q_B$ is the sum of x_1 and g_1 states; concentration of closed reaction centers, $Q_A^- Q_B$ is the sum of x_5 and g_5 states. Q_A^- DCMU designates the occupancy of Q_B site by the inhibitor molecule. The seventh forms with reduced pheophytin are designated as Q_A^- Phe$^-$.

(a) Kinetic curves for DCMU concentrations of 5 and 50 µM. (b) The rate constant of RC chlorophyll reduction was increased from 5×10^3 s^{-1} (curves *1*) to 25×10^3 s^{-1} (curves *2*). Next, the rate constant of nonradiative recombination of Phe$^-$ and P680$^+$ was increased from 2×10^4 s^{-1} (curves *1, 2*) to 10^5 s^{-1} (curves *3*). (c) Kinetic curves obtained with rate constants of nonradiative recombination of Q_A^- and P680$^+$ equal to 400 s^{-1} (curves *1*) and 200 s^{-1} (curves *2*). (d) The initial concentration of PSII states with reduced Q_A^- was increased by 0.1 mM at the expense of diminished concentration of the state with reduced Q_B^-, during the transition from curves *1* to curves *2* with the initial fluorescence level increased by 12.5%.

decreased the stationary fluorescence level (transition from curve *2* to curve *1* Fl).

Both in the absence and presence of DCMU, the rate of the fluorescence increase was affected by the rate constant of RC chlorophyll reduction and the rate constant for nonradiative recombination of Phe$^-$ and P680$^+$ in closed RCs (Fig. 7b). An increase in the rate constant of Phe$^-$ recombination diminished the slope of the fluorescence increase curve in the time range below 100 µs (curve *2* to *3* transition). Upon decreasing the rate constant of electron donation from OEC, e.g., with an assumption of $k_{OEC} = 5000$ s^{-1}, the fluorescence rose without an appreciable first phase (curve *1*). An adequate description of the DCMU-modified fluorescence curve was obtained by assigning a rate constant for Phe$^-$ recombination equal to 10^4 s^{-1}, provided that the

rate constant for electron donation k_{OEC} from OEC ranged between 5000 s^{-1} and 25000 s^{-1}. Thus, the model adequately describes the fluorescence increase both in the absence and presence of DCMU, provided that the rate constant of electron donation from OEC decreases at least fourfold in the presence of DCMU.

Experimental results concerning the initial fluorescence levels in the presence and absence of DCMU are controversial. Schansker et al. [8] did not observe any difference. An 11% increase in F_0 level in the presence of DCMU was experimentally observed and model-simulated by Vredenberg [27]. A similar difference in the initial fluorescence values was obtained in the Lasar's model [15] under assumption that DCMU shifts the equilibrium in the reaction of electron transfer from

Q_A^- to Q_B making this reaction more reversible. Within the framework of our model, this means that the states with reduced Q_B^- would be converted to states with the reduced Q_A^- in the presence of DCMU. The elevated content of Q_A^- produced at the expense of the Q_B^- forms would result in elevation of the initial fluorescence level F_0 (curves *1*, *2*, Fig. 7d).

DISCUSSION OF THE MODELING RESULTS

Experiments with application of a single nanosecond flash and simulation of saturation pulse effects with the PSII model allow the stage-by-stage elucidation of how the light energy absorbed in PSII is utilized for electron transport to the quinone pool and is lost in dissipative processes.

In this study we assumed that application of a nanosecond pulse on the background of weak measuring light would have insignificant effect on the chloroplast compartments, in contrast to the effect of continuous actinic light. As well, the PSII electron transport is assumed to occur under constant pH of the lumen and stroma and under constant electric potential across the membrane. Hence, the effects of a single flash can be described with a reduced model that takes into account electron transfer in the donor and acceptor side of the PSII but neglects some processes caused by continuous long-term illumination in the thylakoid membrane.

We identified the parameters (the lumen and stromal pH, electric potential, and the initial extent of the quinone pool reduction) that ensured the best fit of simulated curves with experimental curves of fluorescence decay (Results, subsection 3.2).

Model analysis of flash-induced events in the vicinity of PSII allowed us to estimate the rate constants that could not be determined with sufficient precision from simulation of continuous light effects because of substantial changes in characteristics of thylakoid compartments under continuous illumination.

Under the action of measuring light, the excitations of PSII reaction centers occur much more slowly than electron transfer from OEC to tyrosine and then to oxidized chlorophyll of RC. Therefore, after instantaneous oxidation of all RC chlorophylls by the saturating flash, the reduction of P680+ by tyrosine proceeds within 1 μs, while slower components of P680+ reduction are determined by electron transfer from OEC. Our model reproduces the retardation of the average rate of P680+ reduction (Fig. 6a). The average rate constant of P680+ reduction was lower than the rate of electron donation from tyrosine (3×10^6–10^9 s^{-1}) but was higher than the fastest rate of tyrosine reduction in the OEC cycle (10^3–3×10^4 s^{-1}). Variations of k_{OEC} in the above range had no effect on the decay phases in the fluorescence induction curve. These phases depended on slower processes of electron transfer into the quinone pool.

In the time scale of tens of microseconds after the flash, "excessive" closed RCs appear. The closed RCs with reduced secondary quinone $Q_B^{(2)-}$ immediately transfer electrons to the pool. The closed RCs with oxidized secondary quinone ($Q_A^- Q_B$) are depleted within hundreds of microseconds during electron transfer to the acceptor side of PSII, where open and closed RCs with reduced secondary quinone ($Q_B^{(2)-}$) are generated (Figs. 6b, 6c). Thus, the model describes the transient redistribution of occupancies of PSII states from non-equilibrium flash-induced excitation state toward the state that characterizes transport processes supported by weak measuring light.

Transfer of the initial energy reserve into the quinone pool during excitation with weak measuring light is accompanied by dissipative losses, i.e., by fluorescence emission and nonradiative recombination of negatively charged acceptors (Phe$^-$, Q_A^-) with positively charged RC chlorophyll (P680+). The model showed that characteristics of these dissipative processes strongly affect the maximal (F_m) and initial (F_0) levels in the fluorescence induction curve. This influence was determined by rate constants of nonradiative dissipation (k_{Phe^-}, $k_{Q_A^-}$) and was investigated theoretically by simulating the flash excitation and weak measuring light modes. We found that dissipative processes for these two excitation modes proceed with two fundamentally different rates. Under the simulation of flash excitation, the rate constants for reactions 42–46 (k_{Phe^-}) and reactions 46–50 ($k_{Q_A^-}$) were found to equal 10^{10} s^{-1} and 10^3 s^{-1}, respectively. These quantities allowed us to estimate a certain set of concentrations for the PSII redox states and use it as the base for modeling the effect of weak measuring light. Applying this initial set to our model, we obtained the optimal fit of theoretical curves to experimental flash-induced fluorescence transients. The quantitatively correct ratio of F_m and F_0 values was obtained by assuming that nonradiative recombination with P680+ is described by the following rate constants: $k_{Phe^-} = 10^5$ s^{-1} and $k_{Q_A^-} = 200$ s^{-1}.

Our model provided estimates for the rate constants of nonradiative recombination accounting for F_m/F_0 values observed in the experiment. Let us compare the results of our study with data known from the literature. It should be noted that the PSII model suggested in [13] does not describe the F_0 level. The most elaborated model of PSII [15] is capable of describing the F_0 level; it deals extensively with dissipative processes and simulates the O–J–P kinetics observed under illumination of PSII membrane preparations with continuous light [9]. However, model [15] pays insufficient attention to the emptying of the Q_B site accompanied by the release of plastoquinol to the membrane phase. This deficiency

may account for the poor description of J–I–P kinetics in the fluorescence induction curve and the physiologically unwarranted ratio of F_0 and F_m.

Using the PSII model, we showed that the rate constants of nonradiative recombination of Phe$^-$ with P680$^+$ in closed RCs are several orders of magnitude higher during response to saturating flash ($\sim 10^{10}$ s^{-1}) than during illumination with measuring light. Thus, our model confirms the proposals put forward by Schreiber and Krieger [4]. Recombination fluorescence is quenched predominantly by nonradiative energy losses at the level of the primary radical pair. Furthermore, the rate of these processes increases with the fluorescence rate until the saturating intensity is reached and becomes comparable with the rate of recombination resulting in chlorophyll excitation. The model also showed that the rate of nonradiative recombination of Phe$^-$ and P680$^+$ has no effect on the initial and final levels of the fluorescence induction curve (F_0) but affects the F_m value.

It is a commonly accepted notion that the rate of chlorophyll reduction in RCs is lower for DCMU-treated samples than for untreated samples. Our model provided suitable simulation of experimental kinetics of the fluorescence yield in DCMU-treated cells, even after omitting the interactions of the inhibitor with the Q_B site (data not shown) in accordance with the commonly accepted approach [13, 15, 27]. However, we preferred to incorporate the inhibitor into the model, which allowed us to perform calculations for the given concentration of the inhibitor without additional changes of the model parameters. This approach, introduced for the first time in this work, allowed simulations for the specified concentration of DCMU. In this case, the mechanism of DCMU action on electron transport in PSII was modeled by the irreversible binding of the inhibitor to the empty site.

CONCLUSION

The kinetic model of PSII describes sequential transitions between the states and kinetics of oxidoreductions of electron carriers in PSII under consecutive changes of illumination regimes whose sequence is defined by the experimental protocol. The initial occupancies of the redox states of PSII are determined by preconditioning of the system (dark adaptation or preillumination). We compared the theoretical fluorescence induction curves, computed by simulation of the pulse treatment, and experimental curves obtained with the measurement protocol comprising the excitation of sample by strong light pulse.

We tested and proved the existing hypotheses [38] concerning the mechanism of light pulse treatment in the absence and presence of DCMU. While devising the illumination protocol in [38], it was assumed that a saturating pulse results in accumulation of redox states P680$^+$ and Q_A^- in the PSII reaction center, while the

subsequent reactions of P680$^+$ reduction and Q_A^- oxidation could be investigated by analyzing the fluorescence increase and decay, respectively. The fluorescence decay is supposedly determined by recombination of Q_A^- with oxidized carriers in the donor side of PSII and by electron transfer from Q_A^- to Q_B [39]. The simulation of saturating light pulse treatment within the framework of PSII model allowed us to analyze and explain the aforementioned electron transport processes in PSII.

According to the model, separate phases of the fluorescence induction curve corresponded to certain changes in occupancies of redox states of the PSII electron carriers. The remarkable features of the experimental protocol, i.e., the short length of the light pulse combined with the long-term measurement of fluorescence transients, allowed us to define "reference points" that were helpful for model improvement. The concentrations of PSII redox states obtained by modeling the illumination regime at a certain time interval were taken as the initial values for modeling of the subsequent illumination regime. Quantitative characteristics of the system—the averaged rate of OEC operation, the rates of nonradiative recombination, the initial reduction state of the quinone pool, stromal pH, etc.— were carefully selected to ensure optimal description of amplitudes and durations of individual stages of the kinetic curve, as well as minimal and maximal fluorescence levels (F_0 and F_m) recorded with thermophilic green algae.

The comparison of fluorescence signals in various samples, combined with the model analysis of these signals, will enable researchers to determine the characteristics of transport processes (rate constants, equilibrium constants, and quantitative characteristics of the chloroplast compartments) occurring in various photosynthesizing organisms.

REFERENCES

1. R. Delosme, Biochim. Biophys. Acta **143**, 1088 (1967).
2. C. R. Ireland, S. P. Long, and N. R. Baker, Planta **160**, 550 (1984).
3. C. Neubauer and U. Schreiber, Z. Naturforsch. **42c**, 1246 (1987).

4. U. Schreiber and A. Krieger, FEBS Lett. **397**, 131 (1996).

5. R. J. Strasser, A. Srivastava, and Govindgee, Photochem. Photobiol. **61**, 32 (1995).

6. R. J. Strasser, M. Tsimilli-Michael, and A. Srivastava, in *Chlorophyll Fluorescence: A Signature of Photosynthesis*, Ed. by G. C. Papageorgiou and Govindjee (Springer, Dordrecht, 2005), pp. 321–362.

7. N. Bukhov, E. Egorova, T. Krendeleva, et al., Photosynth. Res. **70**, 155 (2001).

8. G. Schansker, A. Srivastava, Govindjee, and R. J. Strasser, Funct. Plant Biol. **30**, 785 (2003).

9. P. Pospisil and H. Dau, Photosynth. Res. **65**, 41 (2000).

10. P. D. Laible, W. Zipfel, and T.G. Owens, Biophys. J. **66**, 844 (1994).

11. G. Renger and A. Shulze, Photobiochem. Photobiophys. **9**, 79 (1985).

12. O. Van Kooten, J. F. H. Snel, and W. J. Vredenberg, Photosynth. Res. **9**, 211 (1986).

13. A. Stirbet, Govindjee, B. J. Strasser, and R. J. Strasser, J. Theor. Biol. **193**, 131 (1998).

14. D. Lazar, Biochim. Biophys. Acta **1412**, 1 (1999).

15. D. Lazar, J. Theor. Biol. **220**, 469 (2003).

16. N. G. Bukhov, Kh. G. Damirov, T. G. Dzhibladze, et al., Nauchn. Dokl. Vyssh. Shkoly, Biol. Nauki, No. 4, 28 (1988).

17. V. A. Karavaev and A. K. Kukushkin, Biofizika **38**, 958 (1993).

18. A. Yu. Dubinskii and A. N. Tikhonov, Biofizika **42**, 644 (1997).

19. G. Yu. Riznichenko, G. V. Lebedeva, O. V. Demin, and A. B. Rubin, J. Biol. Phys. **25**, 177 (1999).

20. G. V. Lebedeva, N. E. Belyaeva, G. Yu. Riznichenko, et al., Fiz. Khim. **74**, 1897 (2000).

21. N. E. Belyaeva, Candidate's Dissertation in Mathematical Physics (MGU, Moscow, 2004).

22. G. V. Lebedeva, N. E. Belyaeva, O. V. Demin, et al., Biofizika **47**, 1044 (2002) [Biophysics **47**, 968 (2002)].

23. N. E. Belyaeva, G. V. Lebedeva, and G. Yu. Riznichenko, in *Mathematics, Computer, and Education* (Progress–Traditsiya, Moscow, 2003), Vol. 10, pp. 263-276 [in Russian].

24. A. A. Bulychev, M. M. Niyazova, and A. B. Rubin, Biol. Membrany **4**, 262 (1987).

25. A. A. Bulychev and W. J. Vredenberg, Bioelectrochemistry **54**, 157 (2001).

26. W. J. Vredenberg and A. A. Bulychev, Bioelectrochemistry **60**, 87 (2003).

27. W. J. Vredenberg, in *Chlorophyll Fluorescence: A Signature of Photosynthesis*, Ed. by G. C. Papageorgiou and Govindjee (Springer, Dordrecht, 2005), pp. 133–172.

28. S. A. Kuznetsova, Candidate's Dissertation in Mathematical Physics (MGU, Moscow, 2000).

29. U. Schreiber, U. Schliwa, and W. Bilger, Photosynth. Res. **10**, 51 (1986).

30. G. H. Schatz, H. Brock, and A. R. Holzwarth, Biophys. J. **54**, 397 (1988).

31. W. Leibl, J. Breton, J. Deprez, and H.-W. Trissl, Photosynth. Res. **22**, 257 (1989).

32. T. A. Roelofs, C.-H. Lee, and A. R. Holzwarth, Biophys. J. **61**, 1147 (1992).

33. H. Dau and K. Sauer, Biochim. Biophys. Acta. **1102**, 91 (1992).

34. H. Dau, Photochem. Photobiol. **60**, 1 (1994).

35. K. Gibasiewicz, A. Dobek, J. Breton, and W. Leibl, Biophys. J. **80**, 1617 (2001).

36. J. Lavergne and H.-W. Trissl, Biophys. J. **68**, 2474 (1995).

37. G. Christen, R. Steffen, and G. Renger, FEBS Lett. **475** 103 (2000).

38. R. Steffen, G. Christen, and G. Renger, Biochemistry **40** 173 (2001).

39. G. Christen, A. Seeliger, and G. Renger, Biochemistry **38**, 6082 (1999).

40. A. Laisk and D.A. Walker, Proc. R. Soc. London, Ser. B **237**, 417 (1989).

41. I. A. Reynolds, E. A. Johnson, and C. Tanford, Proc. Natl. Acad. Sci. USA **82**, 6869 (1985).

42. A. B. Hope, R. R. Huilgol, M. Panizza, et al., Biochim. Biophys. Acta **1100**, 15 (1992).